Interpreting the behavior of the NICSzz by resolving in orbitals, sign, and positions

Acke, Guillaume; Van Damme, Sofie; Havenith, Remco W. A.; Bultinck, Patrick

Published in:
Journal of Computational Chemistry

DOI:
10.1002/jcc.25095

Publication date:
2018

Interpreting the behavior of the NICS$_{zz}$ by resolving in orbitals, sign and positions

Guillaume Acke[*, †] Sofie Van Damme[*, †]
Remco W.A. Havenith[*, †, ‡] Patrick Bultinck [*, †, §]

October 17, 2017

Abstract

The zz component of the Nucleus Independent Chemical Shift or the NICS$_{zz}$ is commonly used as a quantifier of the (anti)aromatic character of a (sub)system. One of the underlying assumptions is that a position can be found where the 'aromatic' ring currents are adequately reflected in the corresponding NICS$_{zz}$ value. However, as the NICS$_{zz}$ is the result of an integration over the entire space, it no longer explicitly contains the information needed to quantify the separate contributions arising from underlying current density patterns. In this study, we will show that these contributions can be revealed by resolving the NICS$_{zz}$ into orbitals, sign and positions. Our analysis of benzene in terms of these resolutions shows that the same underlying current density can lead to highly complex shielding patterns that vary greatly depending on the position of the NICS$_{zz}$-probe. As such, our results indicate that any analysis solely based on NICS$_{zz}$-values can lead to results that are difficult to interpret, even if the system under study is considered to be well-known.

Keywords: NICSzz, NICSDzz, Shielding Density Field

[*]Ghent Quantum Chemistry Group, Department of Inorganic and Physical Chemistry, Faculty of Science, Ghent University, Faculty of Science, Krijgslaan 281, S3, 9000 Ghent, Belgium

[†]Members of the QCMM alliance Ghent-Brussels

[‡]Theoretical Chemistry, Zernike Institute for Advanced Materials and Stratingh Institute for Chemistry, University of Groningen, 9747 AG Groningen, The Netherlands

[§]Corresponding Author : Patrick.Bultinck@Ugent.Be

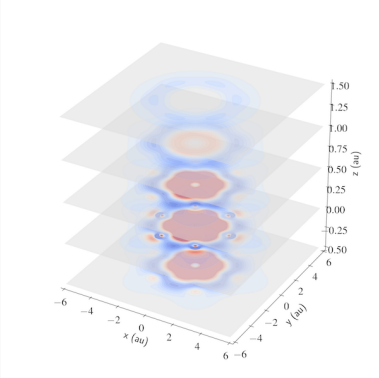

The zz component of the Nucleus Independent Chemical Shift or the NICS_{zz} is commonly used as a quantifier of (anti)aromaticity. Given that a NICS_{zz}-value is only a single scalar value, the interpretation of the NICS_{zz} in terms of the underlying current density patterns is not straightforward. In this paper, we will show that relevant contributions can be revealed by resolving the NICS_{zz} into orbitals, sign and positions.

INTRODUCTION

Although the term 'aromaticity' has become common in chemical thought, finding a theoretical correspondence starting from quantum mechanics has proven difficult[1]. Currently, a multitude of criteria exist[2–13], which do not always lead to the same conclusions[2,14–19]. One of these criteria is the magnetic criterion, which is based on London's observation that an unsaturated ring can sustain an induced ring current in the presence of a uniform magnetic field perpendicular to the molecular plane[20]. The quantum chemical calculation of these ring current densities was made possible by, among others, the contributions from Pople and Keith and Bader[21,22].

Once such a current density has been calculated, it can be analyzed for aromatic behavior in two ways[23]. On the one hand, the induced current density may be evaluated directly, typically by visualizing the vector fields itself[24–26]. On the other hand, indirect quantities such as magnetic shielding[3], magnetizability[27,28] and chemical shifts[29,30] can be derived from the underlying current density[6]. Of these quantities, the 'Nucleus Independent Chemical Shift' or the NICS is one of the most popular criteria[3,31].

The NICS is usually sampled with a probe or "ghost atom" at a single reference position $\boldsymbol{r}_R$ and corresponds to the (scaled) negative of the trace of the magnetic shielding density tensor $\boldsymbol{\sigma}(\boldsymbol{r}_R)$[3]. Although, for aromatic monocyclic compounds, the probe was originally positioned at the center of the ring, concerns about the contributions of shielding density components that are not implied in the phenomenon of aromaticity have spurred the development of variants of the NICS. Common approaches include varying the position of the probe, selecting only one component of the shielding density tensor, and/or dissecting the NICS into its orbital contributions[32–34]. Of these approaches, the combination of selecting only the zz-component of the NICS and sampling at 1 Å above the ring center has gained popularity. It is common to denote any NICS sampled at a given vertical distance x Å to the molecular plane as NICS(x), with the distance x in round brackets. As such, the most popular NICS_{zz} descriptor[31,32] is designated as NICS(1).

The underlying assumption that all information concerning aromatic character can be reflected by a single measure has been criticized severely[4,23,25,35–38]. In an attempt to address

this criticism, 2-dimensional NICS scans[39–41] and 3-dimensional contour surfaces of the NICS and related magnetic indices[42–46] have been designed. As we have shown recently[47], an important observation in this respect is that there exist many-to-one mappings between ring current densities and NICS$_{zz}$-values. This is a direct consequence of the fact that the NICS$_{zz}$ tries to reduce the complicated magnetic behavior of the system to a single number. Moreover, contrary to intuition, increasing the number of points in which the NICS$_{zz}$ is sampled does not alleviate this problem[47].

Given that the NICS$_{zz}$ is a single scalar value, the interpretation of the NICS$_{zz}$-value in terms of this current density is not straightforward. As such, it remains unclear which parts of the current density influence the value of the NICS$_{zz}$ sampled at a certain position and to what extent.

Jameson and Buckingham noted that the magnetic shielding tensor $\boldsymbol{\sigma}(\boldsymbol{r}_R)$ at a reference position $\boldsymbol{r}_R$ is obtained by integrating the magnetic shielding density tensor $\boldsymbol{\Sigma}(\boldsymbol{r};\boldsymbol{r}_R)$[48,49]

$$\boldsymbol{\sigma}(\boldsymbol{r}_R) = \int \boldsymbol{\Sigma}(\boldsymbol{r};\boldsymbol{r}_R)\mathrm{d}\boldsymbol{r} \ . \tag{1}$$

As was shown by Lazzeretti and coworkers in the context of nuclear shieldings, the resulting shielding density function are useful to determine regions where shielding-deshielding mechanisms take place and to analyze the contribution by different domains of the current density[50–54]. In the theoretical section, we will exploit the relation of the NICS to $\boldsymbol{\sigma}$ to define the 'Nucleus Independent Chemical Shift Density' or the NICSD (and its zz-component, the NICSD$_{zz}$)

$$\mathrm{NICS}(\boldsymbol{r}_R) = \int \mathrm{NICSD}(\boldsymbol{r};\boldsymbol{r}_R)\mathrm{d}\boldsymbol{r} \ , \tag{2}$$

which resolves the NICS in space. By combining this NICSD$_{zz}$ with resolutions into orbitals and/or sign, we obtain quantities that express the contributions of relevant current density patterns to the NICS$_{zz}$.

METHODOLOGY

Theory

In order to clearly indicate the relation between the NICS$_{zz}$ and its resolutions, we will briefly review the necessary theoretical constructs as introduced by Jameson and Buckingham[48,49]. A current density vector field $\boldsymbol{J}^{\boldsymbol{B}^{\text{ext}}}(\boldsymbol{r})$ is magnetically induced by a uniform external magnetic vector field $\boldsymbol{B}^{\text{ext}}$. As described in the law of Biot-Savart, this induced field $\boldsymbol{J}^{\boldsymbol{B}^{\text{ext}}}(\boldsymbol{r})$ determines the induced magnetic vector field $\boldsymbol{B}^{\text{ind}}(\boldsymbol{r}_R)$ at a reference position $\boldsymbol{r}_R$[55]

$$\boldsymbol{B}^{\text{ind}}(\boldsymbol{r}_R) = \int \frac{\mu_0}{4\pi} \frac{\boldsymbol{J}^{\boldsymbol{B}^{\text{ext}}}(\boldsymbol{r}) \times (\boldsymbol{r}_R - \boldsymbol{r})}{\|\boldsymbol{r}_R - \boldsymbol{r}\|^3} \mathrm{d}\boldsymbol{r} \ , \tag{3}$$

with μ_0 the permeability of free space. The induced magnetic vector field $\boldsymbol{B}^{\text{ind}}(\boldsymbol{r}_R)$ at the reference position $\boldsymbol{r}_R$ is related to the uniform external magnetic vector field $\boldsymbol{B}^{\text{ext}}$ through the magnetic shielding tensor field $\boldsymbol{\sigma}(\boldsymbol{r}_R)$

$$\boldsymbol{B}^{\text{ind}}(\boldsymbol{r}_R) = -\boldsymbol{\sigma}(\boldsymbol{r}_R) \cdot \boldsymbol{B}^{\text{ext}} \ , \tag{4}$$

where $\boldsymbol{\sigma}(\boldsymbol{r}_R)$ is given by

$$\sigma_{\alpha\delta}(\boldsymbol{r}_R) = -\int \frac{\mu_0}{4\pi} \epsilon_{\alpha\beta\gamma} \frac{(r_{R\beta} - r_\beta)}{\|\boldsymbol{r}_R - \boldsymbol{r}\|^3} \mathcal{J}_\gamma^{B^{\text{ext},\delta}}(\boldsymbol{r}) \mathrm{d}\boldsymbol{r} \ , \tag{5}$$

with $\epsilon_{\alpha\beta\gamma}$ the Levi-Civita tensor with implied Einstein summation and $\mathcal{J}_\gamma^{B^{\text{ext},\delta}}(\boldsymbol{r})$ the γ-component of the current density tensor

$$\mathcal{J}_\gamma^{B^{\text{ext},\delta}}(\boldsymbol{r}) = \frac{\partial}{\partial B_\delta^{\text{ext}}} J_\gamma^{\boldsymbol{B}^{\text{ext}}}(\boldsymbol{r}) \ . \tag{6}$$

The quantity inside the integrand of equation (5) is called the (Jameson-Buckingham) magnetic shielding density tensor field $\boldsymbol{\Sigma}$[52,56,57]. From equation (5) it follows that the zz-component of this tensor field is given by

$$\Sigma_{zz}(\boldsymbol{r}; \boldsymbol{r}_R) = -\frac{\mu_0}{4\pi} \frac{(r_{Ry} - r_y)\mathcal{J}_x^{B^{\text{ext},z}}(\boldsymbol{r}) - (r_{Rx} - r_x)\mathcal{J}_y^{B^{\text{ext},z}}(\boldsymbol{r})}{\|\boldsymbol{r}_R - \boldsymbol{r}\|^3} \ . \tag{7}$$

By determining $\boldsymbol{\sigma}$ at the nuclei in the nuclear framework, we can obtain theoretical predictions for experimentally measurable magnetic shieldings. In the NICS-methodology, a virtual core is used, which does not influence the shielding itself and which allows one to probe the

entire induced magnetic field. The underlying idea is that there exist reference positions for which the magnetic shielding of this probe provide correspondences with the phenomena of aromaticity and anti-aromaticity. Furthermore, in order to enhance the correspondence with NMR chemical shifts, the NICS is defined as the (scaled) negative trace of $\boldsymbol{\sigma}$

$$\mathrm{NICS}(\boldsymbol{r}_R) = -\frac{1}{3}\left[\sigma_{xx}(\boldsymbol{r}_R) + \sigma_{yy}(\boldsymbol{r}_R) + \sigma_{zz}(\boldsymbol{r}_R)\right] \ . \tag{8}$$

The associated NICS_{zz} is equal to the negative $\sigma_{zz}(\boldsymbol{r}_R)$ component.

In the spirit of the ideas of Jameson and Buckingham, we can define the 'Nucleus Independent Chemical Shift Density' or the NICSD as

$$\mathrm{NICSD}(\boldsymbol{r};\boldsymbol{r}_R) = -\frac{1}{3}\left[\Sigma_{xx}(\boldsymbol{r};\boldsymbol{r}_R) + \Sigma_{yy}(\boldsymbol{r};\boldsymbol{r}_R) + \Sigma_{zz}(\boldsymbol{r};\boldsymbol{r}_R)\right] \ , \tag{9}$$

and its associated zz-component $\mathrm{NICSD}_{zz}(\boldsymbol{r};\boldsymbol{r}_R)$

$$\mathrm{NICSD}_{zz}(\boldsymbol{r};\boldsymbol{r}_R) = \frac{\mu_0}{4\pi}\frac{(r_{Ry}-r_y)\mathcal{J}_x^{B^{\mathrm{ext},z}}(\boldsymbol{r}) - (r_{Rx}-r_x)\mathcal{J}_y^{B^{\mathrm{ext},z}}(\boldsymbol{r})}{\|\boldsymbol{r}_R-\boldsymbol{r}\|^3} \ . \tag{10}$$

An immediate consequence of using this underlying scalar density field is that we can separate this field into its shielding (negative) and deshielding (positive) contributions by sign resolving the field

$$\mathrm{NICSD}^{-}_{zz}(\boldsymbol{r};\boldsymbol{r}_R) = \mathrm{NICSD}_{zz}(\boldsymbol{r};\boldsymbol{r}_R)\delta\left[\mathrm{NICSD}_{zz}(\boldsymbol{r};\boldsymbol{r}_R) < 0\right] \tag{11}$$

$$\mathrm{NICSD}^{+}_{zz}(\boldsymbol{r};\boldsymbol{r}_R) = \mathrm{NICSD}_{zz}(\boldsymbol{r};\boldsymbol{r}_R)\delta\left[\mathrm{NICSD}_{zz}(\boldsymbol{r};\boldsymbol{r}_R) > 0\right] \ , \tag{12}$$

where δ denotes a generalized Dirac delta function, which is equal to one only if the condition inside square brackets is satisfied. We note that we can also define the sign-resolved NICS^{-}_{zz} and NICS^{+}_{zz} by integrating over their respective sign-resolved NICSD^{-}_{zz} and NICSD^{+}_{zz}-fields

$$\mathrm{NICS}^{\pm}_{zz}(\boldsymbol{r}_R) = \int \mathrm{NICSD}^{\pm}_{zz}(\boldsymbol{r};\boldsymbol{r}_R)\mathrm{d}\boldsymbol{r} \ . \tag{13}$$

A decomposition of the current density tensor into its orbital contributions can also be echoed in the NICSD_{zz}. In line with the research done by Steiner and Fowler[58], the ipsocentric gauge distribution of the CTOCD-DZ method allows the total current density tensor to be decomposed as the sum of orbital contributions. For the aromatic system we will study (benzene), three orbital-subsystems are conventionally taken into account: the inner shells

(core), the σ system and the π system. For each of these orbital-resolved currents, we can define an associated orbital resolved NICSD$_{zz}$-field, in this case NICSD$^{\text{core}}_{zz}$, NICSD$^{\sigma}_{zz}$ and NICSD$^{\pi}_{zz}$. For instance, the NICSD$^{\pi}_{zz}$ can be defined as

$$\text{NICSD}^{\pi}_{zz}(\boldsymbol{r};\boldsymbol{r}_R) = \frac{\mu_0}{4\pi}\frac{(r_{Ry}-r_y)\mathcal{J}_x^{B^{\text{ext},z},\pi}(\boldsymbol{r}) - (r_{Rx}-r_x)\mathcal{J}_y^{B^{\text{ext},z},\pi}(\boldsymbol{r})}{\|\boldsymbol{r}_R-\boldsymbol{r}\|^3}\,, \tag{14}$$

with $\mathcal{J}^{B^{\text{ext},z},\pi}$ the current density tensor associated with the π-system consisting of the sum of all π-orbital contributions.

$$\mathcal{J}^{B^{\text{ext},z},\pi} = \sum_{n\in\pi}\mathcal{J}^{B^{\text{ext},z},n} \tag{15}$$

We note that we can again sign-resolve these fields into NICSD$^{\text{core},\pm}_{zz}$, NICSD$^{\sigma,\pm}_{zz}$, NICSD$^{\pi,\pm}_{zz}$ (see equation 12) and that we can obtain the sign-resolved NICS$^{\pm}_{zz}$ by integrating over these fields NICS$^{\text{core},\pm}_{zz}$, NICS$^{\sigma,\pm}_{zz}$, and NICS$^{\pi,\pm}_{zz}$ (see equation 13).

Computational details

We fully optimized benzene at the Hartree-Fock level with the 6-311g(d) basis set with the Gaussian16 code[59], followed by analytical frequency calculations to ensure a true minimum. We calculated the ipso-centric current density maps[24,58] at the coupled perturbed Hartree-Fock level in the 6-311g+(d) basis, using the GAMESS-UK package[60] linked to SYSMO[61]. The resulting current density was specified on a regular grid, centered on the molecular center of benzene, with a width of 12 au and a step size of $\frac{1}{12}$ au, in accordance with the fine grid implemented in the Gaussian16 standalone utility cubegen. All visualizations were obtained by interfacing with the Matplotlib Python package[62]. We note that all (non-orbital resolved) NICSD$_{\alpha\beta}$-fields, with $\{\alpha,\beta\} = \{x,y,z\}$, can also be obtained in Gaussian cube format by passing the appropriate 'ShieldingDensity' keyword to the cubegen utility, which is included in Gaussian16.

RESULTS AND DISCUSSION

In this section, we will apply the framework derived in the theoretical section to the study of benzene, a prototypical aromatic molecule. In order to relate the behavior of the NICS$_{zz}$ at

different reference positions, we will use the scan methodology introduced by Stanger[40,41], where the reference position is set at regular intervals along either the x, y, or z-axis. The orientation of these axes with respect to the benzene molecule is depicted in figure 1.

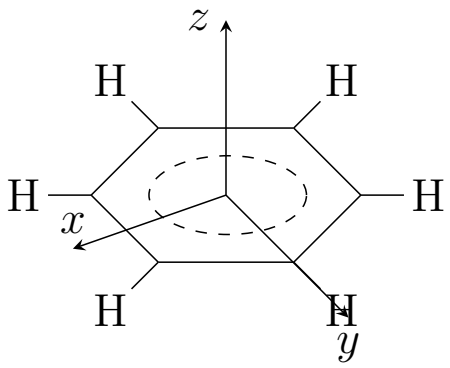

Figure 1: Orientation of the x, y, and z axis relative to the benzene model.

Z-scan

It has already been widely discussed in the literature that the $NICS_{zz}$ does not depend purely on the π system but also on other magnetic shielding contributions due to local circulations of electrons in σ-bonds, lone pairs and core electrons[6,25,63]. A widely accepted technique to reduce the contribution of the σ and core orbital systems is increasing the distance from the probe to the center of benzene, since the effects of the π orbital system are assumed to taper off at a much slower rate[41]. Such reasoning has lead to the recommendation of moving the probe to a distance of 1 Å (1.88 au) above the ring center, where the π orbitals have their maximum density[31]. It is assumed that at this height the induced magnetic field as measured by the $NICS_{zz}$ is made up primarily of contributions of the π system.

The orbital-resolved $NICS_{zz}$ along the z axis seems to support this reasoning (Fig. 2(a)). Around 1 Å (1.88 au) the contributions of the orbital resolved $NICS^{\sigma}_{zz}$ and $NICS^{\text{core}}_{zz}$ are negligible, rendering the $NICS_{zz}$ essentially equal to the $NICS^{\pi}_{zz}$. However, if we resolve these orbital contributions in sign (Fig. 2(b)), we observe that a negligible $NICS^{\sigma}_{zz}$ contribution does *not* indicate that the σ system has no impact on the $NICS_{zz}$ value; rather, it indicates that the $NICS^{\sigma,+}_{zz}$ and $NICS^{\sigma,-}_{zz}$ contributions happen to cancel each other at that height.

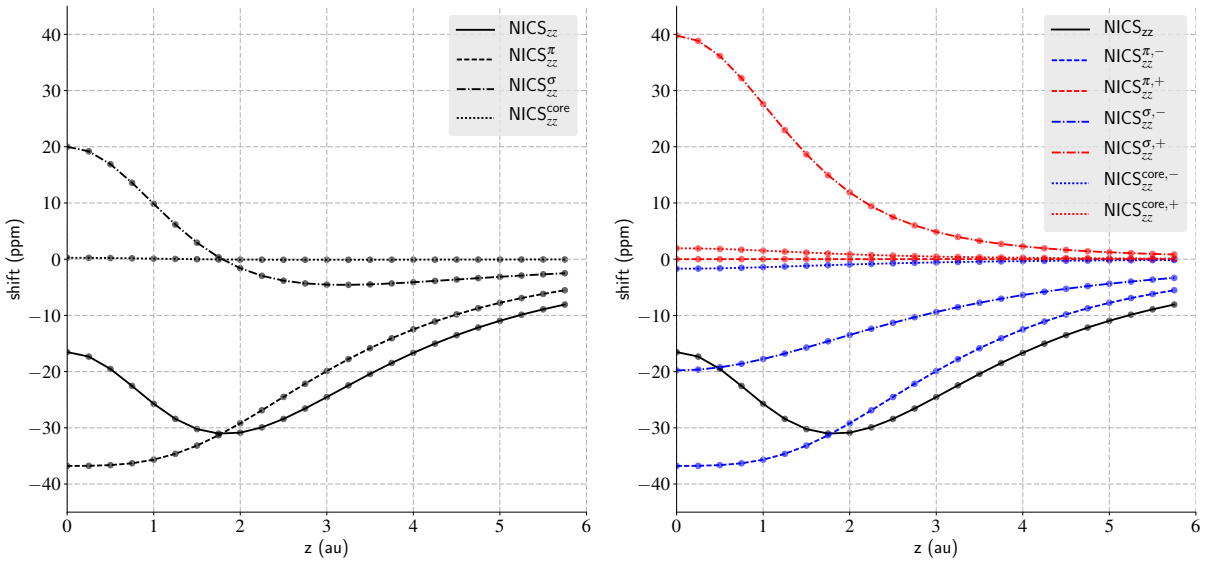

(a) Orbital resolved.

(b) Orbital and sign resolved.

Figure 2: Z-scan of the NICS$_{zz}$ with reference points sampled at $\boldsymbol{r}_R = (0.0, 0.0, r_{Rz})$.

This cancellation is the result of the NICS$^{\sigma,+}_{zz}$ contribution dying of at a much faster rate than the NICS$^{\sigma,-}_{zz}$ contribution. The latter continues to have a non-negligible contribution at large heights above the molecular plane, indicating that σ contributions are *not* short-ranged. Furthermore, although the NICS$^{\text{core}}_{zz}$ contribution is essentially zero over the entire range of the scan, its sign resolution shows that this value consists of two separate contributions when close to the molecular plane. As such, a NICS$_{zz}$ contribution that remains constant can hide a different (sign-resolved) behavior.

We can gain more insight into these results if we inspect the NICS$_{zz}$ associated density field, the NICSD$_{zz}$. As this is a three-dimensional scalar field, we will visualize this field using several plotting planes, the orientation of which is illustrated in Fig. 3. In each cut-plane, the NICSD$_{zz}$-field is visualized using a diverging colormap, with negative values in blue and positive values in red, where the maximum and minimum values are capped at 1 and -1 ppm respectively. To aid visualization, isocontour lines are also plotted at $\pm 10^i$ with $i \in \{3, 2, \ldots, -3, -4\}$. The NICSD$_{zz}$ profiles are given for the total current density as well as for the orbital resolved current densities in figure 4. Fig. 4(a) depicts the fields for a probe positioned in the molecular plane (or $\mathbf{r}_R = (0.0, 0.0, 0.0)$) whereas Fig. 4(b) contains the fields for a probe positioned at $\mathbf{r}_R = (0.0, 0.0, 2.0$ au). These profiles reveal

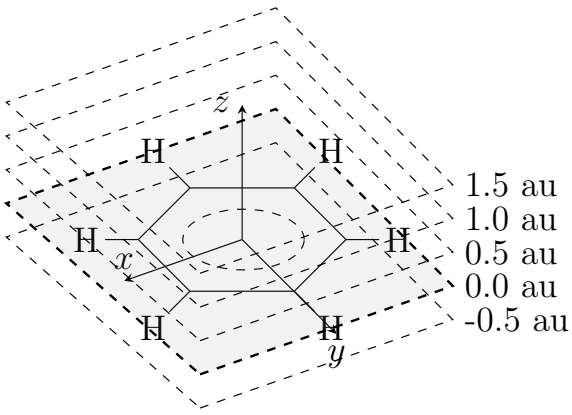

Figure 3: Orientation of cut planes trough the NICSD fields.

that intricate density profiles give rise to the $NICS_{zz}$ with non-negligible contributions from many regions that are traditionally not associated with aromaticity. As such, the negligible contribution of the $NICS_{zz}^{core}$ is built up from six local atomic circulation that give rise to shielding and deshielding spikes of similar magnitude[50]. These shielding and deshielding spikes are proportionally reduced by increasing the height from the molecular plane.

The lack of positive contributions to the $NICS_{zz}^{\pi}$ is reflected in the $NICSD_{zz}^{\pi}$. Another striking feature is that although both π ring-currents on either side of the molecular plane are reflected in the $NICSD_{zz}^{\pi}$ field, an increase in the height of the probe leads to a drastic reduction in the shielding density associated with the lower ring-current. This gives an indication why no minimum can be found in the scan profile of the $NICS_{zz}^{\pi}$, despite the probe being placed closer to the density of the upper π ring-current. This interpretation seems to be in line with the studies of Juselius and Sundholm[64] and Pelloni and Lazzeretti[65], where the (single) ring current model is shown to yield insight into the $NICS_{zz}^{\pi}$-value for high probe positions.

The $NICSD_{zz}^{\sigma}$ is highly complex, with features from both the carbon-carbon and carbon-hydrogen bonds. Furthermore, these features have contributions even at high altitudes above the molecular plane. Most importantly, the features of the σ system remain clearly visible in the $NICSD_{zz}$ profile, even if the distance of the probe to the molecular plane is increased.

We can reduce the complexity contained in the $NICSD_{zz}$ by integrating over 'slices' of space, with each slice a rectangular volume parallel to the xy-plane with a thickness of

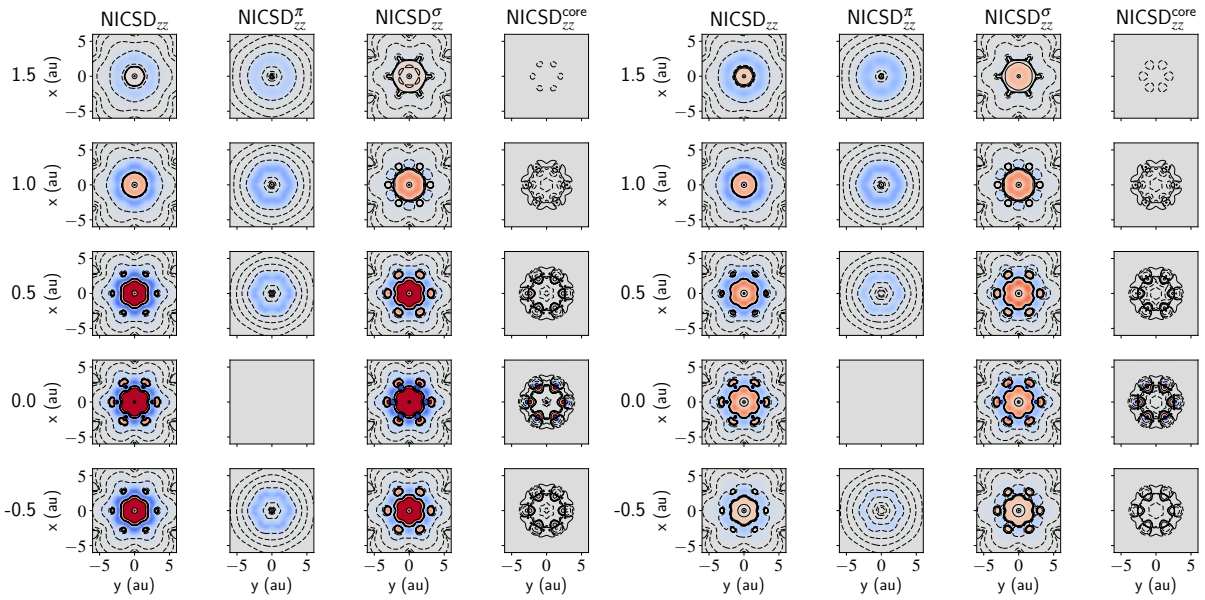

(a) $\boldsymbol{r}_R$ = (0.0, 0.0, 0.0) (au)

(b) $\boldsymbol{r}_R$ = (0.0, 0.0, 2.0) (au)

Figure 4: Collection of cut planes at $\mathbf{r}_z$ =-0.5, 0.0, 0.5, 1.0 and 1.5 au, through the NICSD$_{zz}$ field, equation 10, and the orbital resolved variants, as in equation 14, associated with probes positioned along the z-axis at (0,0,$\mathbf{r}_{Rz}$). Blue regions indicate negative shielding contributions, whereas red regions indicate positive shielding contributions. Dashed contour lines denote negative values, solid contour lines positive values. Contour values are plotted at $\pm 10^i$ with $i \in \{3, 2, \ldots, -3, -4\}$

$\Delta = \frac{1}{12}$ au. As such, the shift contribution NICS$^{z,\Delta}_{zz}(h)$ of such a slice at a given height h is given by

$$\text{NICS}^{z,\Delta}_{zz}(h) = \int_{h-\frac{\Delta}{2}}^{h+\frac{\Delta}{2}} \mathrm{d}r_z \int_{-\infty}^{+\infty} \mathrm{d}r_y \int_{-\infty}^{+\infty} \mathrm{d}r_x \text{NICSD}_{zz}(\boldsymbol{r}; \boldsymbol{r}_R) \ . \tag{16}$$

If we divide space into such non-overlapping slices, centered at evenly spaced positions with an interval of $\frac{1}{12}$ au, we obtain the results depicted in Fig. 5. These plots confirm that the contribution of the lower half of the π system is drastically reduced by increasing the height of the probe. They also indicate that the regions of maximum density of the π system have the largest contributions; however, non-negligible contributions occur up to and beyond heights of 4 au above and below the molecular plane. We note that the σ system also has non-negligible contributions that extend above the height where the π system has

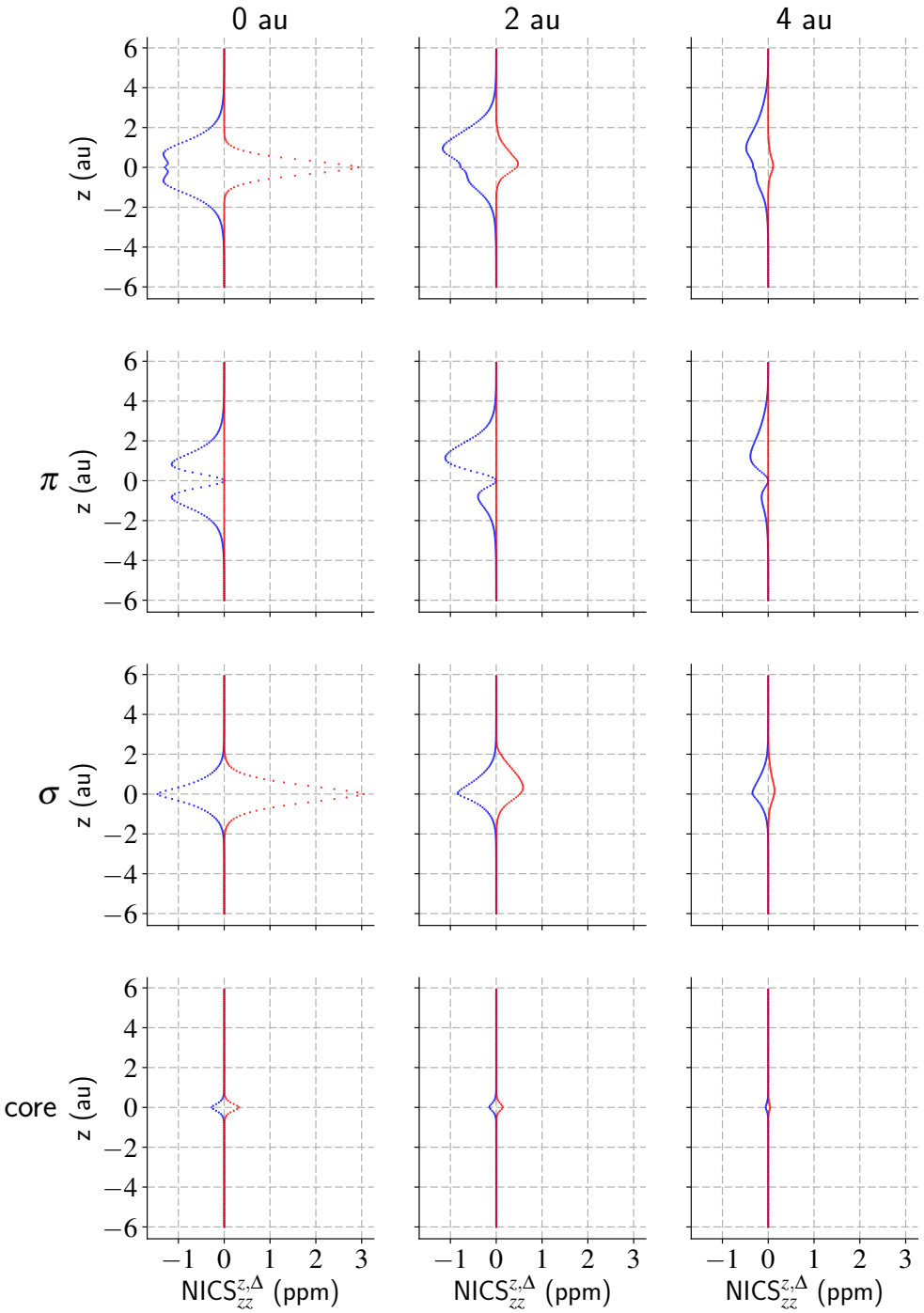

Figure 5: The $\mathrm{NICS}^{z,\Delta}_{zz}(h)$ shift contribution, equation 16, for non-overlapping slices parallel to the xy-plane at a height h with a thickness of $\Delta = \frac{1}{12}$ au, centered on regularly spaced points with an interval of $\frac{1}{12}$ au. At each height h, the contributions are sign-resolved into negative (blue) and positive (red) contributions. The $\mathbf{r}_{Rz}$ coordinate of the probe is given in the respective headings.

its maximum density.

X-scan

In order to identify 'local' and 'global' currents, Gershoni-Poranne and Stanger[41] devised the XY-scan methodology, where the NICS-probes are placed along the x and y axes of a given compound (see Fig. 1 for the orientation of those axes). In an attempt to reduce the σ contributions in the NICS$_{zz}$, they performed a series of scans at different heights above the molecular plane. At a minimal height of 1.7 Å (3.2 au) the σ effects were no longer considered as significant, primarily based on the absence of a pronounced minimum over the carbon-carbon bond and the (qualitative) similarity with the NICS$^{\pi}_{zz}$ profile.

If we compare the x-scan profiles of the orbital and sign resolved NICS$_{zz}$ in the molecular plane (Fig. 6) and at a height of 3.5 au (Fig. 7), we notice that the NICS$^{\sigma}_{zz}$ has a minimum above the carbon-carbon bond at both heights, but that this minimum is not reflected in the NICS$_{zz}$ at 3.5 au. However, the lack of a minimum in the NICS$_{zz}$ profile does *not* indicate that the contributions of the NICS$^{\sigma}_{zz}$ are no longer significant along the entire range of the x-scan. Indeed, although the NICS$^{\pi}_{zz}$ profile mirrors the NICS$_{zz}$ profile qualitatively at a height of 3.5 au, the NICS$^{\sigma}_{zz}$ has larger sign-resolved contributions than those of the NICS$^{\pi}_{zz}$ when moving beyond 4 au in the x-direction. We also remark that, in contrast to the z-scan profile, the NICS$^{\pi;+}_{zz}$ no longer remains negligible along the scan, with rising contributions starting around the carbon-carbon bond. As mentioned by Stanger[41], for the π-system this behavior is, in rough approximation, in line with the Biot-Savart law for induced currents within circular loops. However, the behavior of the σ-system is far more intricate and cannot be describe adequately by means of such simple models, even for a prototypical molecule such as benzene.

However, we can gain more insight into this behavior by investigating the underlying NICSD$_{zz}$-fields (Fig. 8), where the probe is sampled on two positions along the x-axis in the molecular plane. These plots reveal that, in contrast to the z-scan, the underlying shielding densities have very different shielding patterns depending on the position of the probe. In the case of the π-system, if we move along the x-axis, the probe is gradually deshielded, since the (same) underlying diamagnetic π-current is reflected to different extents in the NICSD$^{\pi;+}_{zz}$- and NICSD$^{\pi;-}_{zz}$-fields. Due to this behavior, we note that negative (positive) shielding values

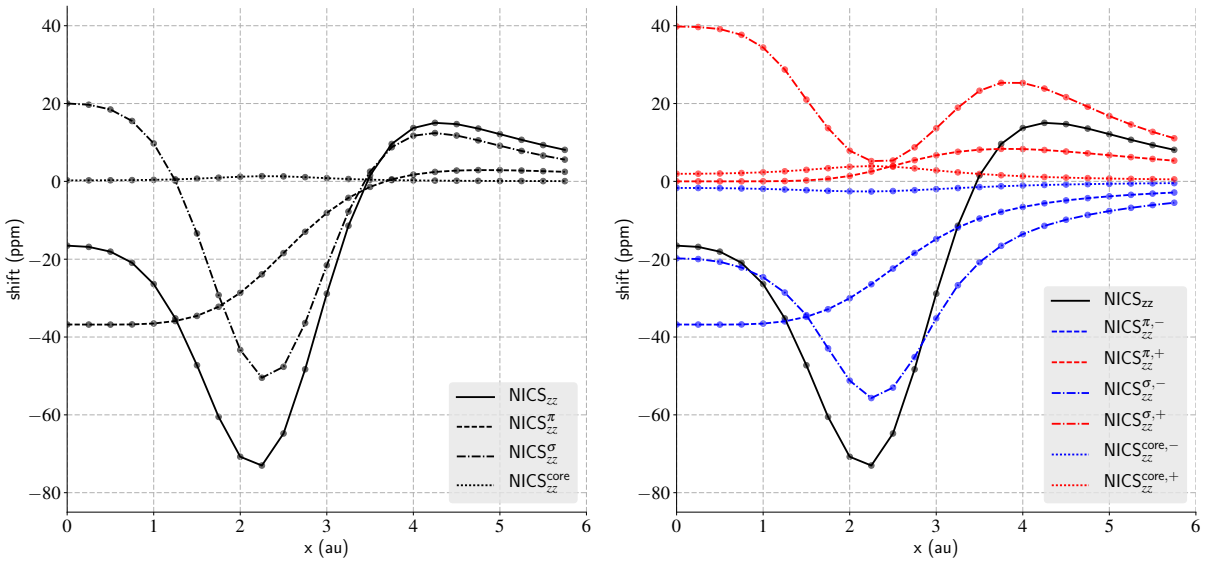

(a) Orbital resolved.

(b) Orbital and sign resolved.

Figure 6: X-scan of the NICS$_{zz}$ with reference points sampled at $\boldsymbol{r}_R$=(r_{Rx}, 0, 0) (au).

can no longer be directly related to the presence of induced diatropic (paratropic) ring currents or "aromaticity" ("antiaromaticity").

We can again try to reduce the complexity contained in these plots by integrating over 'slices' of space, with each slice now oriented along the yz-plane with a thickness of $\Delta = \frac{1}{12}$ au (Fig. 9). As such, the shift contribution NICS$^{x,\Delta}_{zz}(d)$ of such a slice at a given distance d along the x-axis is given by

$$\text{NICS}^{x,\Delta}_{zz}(d) = \int_{d-\frac{\Delta}{2}}^{d+\frac{\Delta}{2}} \mathrm{d}r_x \int_{-\infty}^{+\infty} \mathrm{d}r_z \int_{-\infty}^{+\infty} \mathrm{d}r_y \text{NICSD}_{zz}(\boldsymbol{r}; \boldsymbol{r}_R) \ . \tag{17}$$

When sampling the probes in the molecular plane, the NICS$_{zz}$ profile has the largest similarity with the NICS$^{\sigma}_{zz}$, whereas sampling at a height of 3.5 au, the NICS$_{zz}$ profile has the largest similarity with the NICS$^{\pi}_{zz}$. This provides quantitative support for the findings of Stanger[41], who reported a greater qualitative similarity between the NICS$_{zz}$ and the NICS$^{\pi}_{zz}$ at larger heights above the molecular plane.

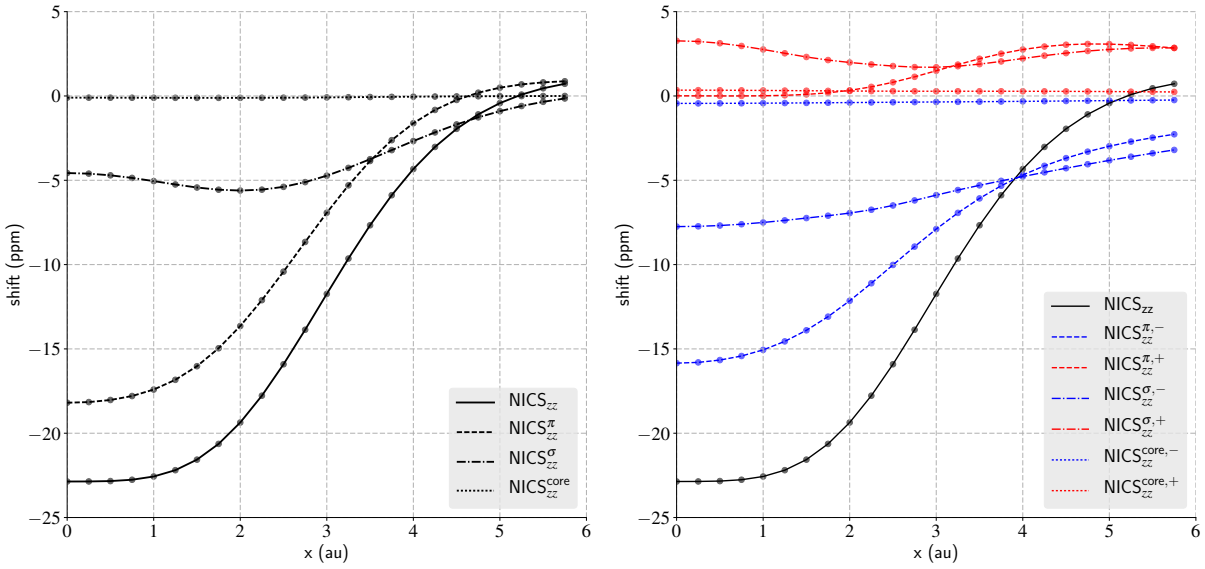

(a) Orbital resolved.

(b) Orbital and sign resolved.

Figure 7: X-scan of the NICS$_{zz}$ with reference points sampled at r_R=(r_{Rx}, 0, 3.5) (au).

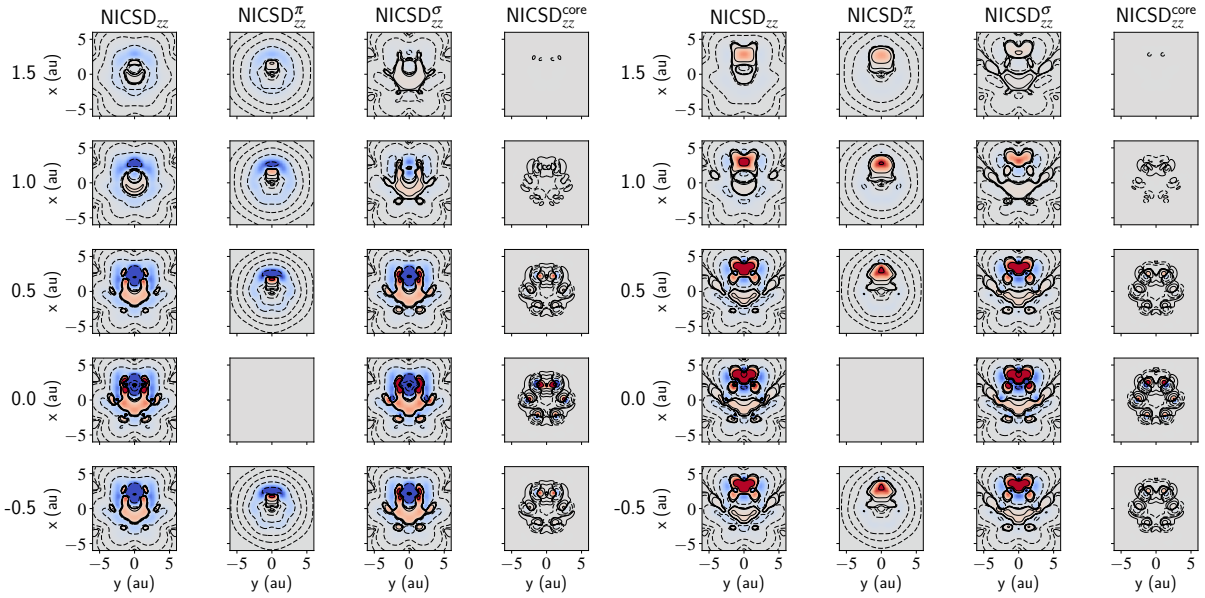

(a) $\mathbf{r}_R$ = (2.0, 0.0, 0.0) (au)

(b) $\mathbf{r}_R$ = (4.0, 0.0, 0.0) (au)

Figure 8: Collection of cut planes, at $\mathbf{r}_z$=-0.5, 0.0, 0.5, 1.0 and 1.5 au, through the NICSD$_{zz}$ field, equation 10, and the constituent orbital resolved NICSD$_{zz}$ field, as in equation 14, associated with probes positioned along the x-axis in the molecular plane (with positions mentioned in the captions (a) and (b)). See figure 4 caption for other details.

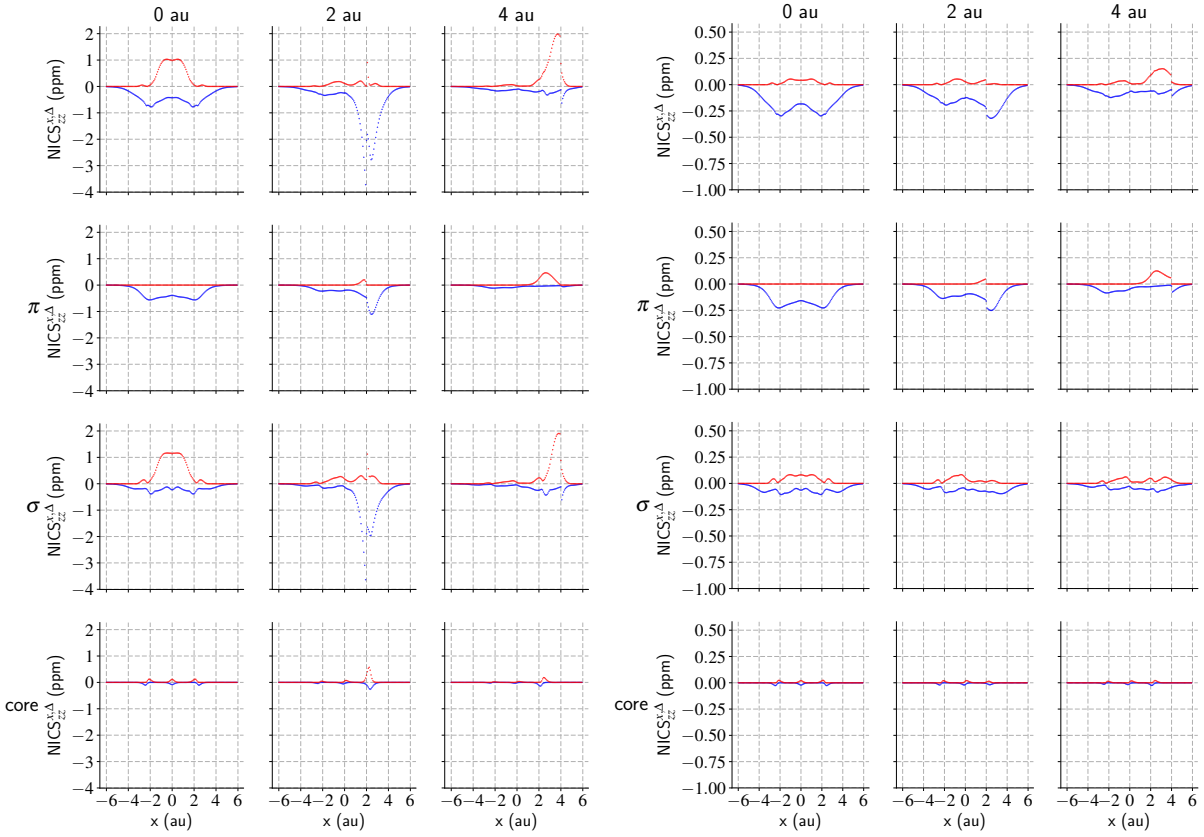

(a) Probes sampled in the molecular plane.

(b) Probes sampled at a height of 3.5 au.

Figure 9: The $\mathrm{NICS}_{zz}^{x,\Delta}(d)$ shift contribution, equation 17, for non-overlapping slices parallel to the yz-plane with a thickness of $\Delta = \frac{1}{12}$ au, centered on regularly spaced points with an interval of $\frac{1}{12}$ au. At each d-value, the contributions are sign-resolved into negative (blue) and positive (red) contributions. The position of the probe is given in the respective headings.

CONCLUSIONS

In this study, we have shown that resolving the $NICS_{zz}$ into orbitals, sign, and positions allows us to gain more insight into its behavior in terms of resolved shielding contributions. We have shown that for benzene, the $NICS_{zz}$-value is made up of contributions from all current density patterns present. Increasing the height of the probe relative to the molecular plane invariably decreases the contributions of the π system and, contrary to widespread perception, does not unambiguously increase its relative contribution. Our analysis also shows that a negligible $NICS_{zz}$-value does not necessarily indicate that the system behind this contribution does not play any role in the behavior of the $NICS_{zz}$. Indeed, the current density associated with a certain system can be reflected in highly complicated shielding patterns that happen to integrate to zero. Furthermore, that same current density can lead to very different shielding patterns depending on the position of the probe. These complicating features indicate that any analysis solely based on $NICS_{zz}$-values can lead to results that are difficult to interpret, even if the system under study is considered to be well-known.

ACKNOWLEDGMENTS

All authors acknowledge financial support form the Research Foundation Flanders (FWO-Vlaanderen) for continuous support. Dr. Amnon Stanger (Technion, Israel Institute of Technology) and dr. Peter B. Karadakov (The University of York) are gratefully acknowledged for their useful suggestions and discussions.

References

1. Krygowski, T. M., Cyranski, M. K., Czarnocki, Z., Häfelinger, G. and Katritzky, A. R. *Tetrahedron* **2000**, *56*, 1783–1796.

2. Cyranski, M., Krygowski, T. M., Katritzky, A. and Schleyer, P. v. R. *J. Org. Chem.* **2002**, *67*, 1333–1338.

3. Schleyer, P. v. R., Maerker, C., Dransfeld, A., Jiao, H. and Hommes, N. J. v. E. *J. Am. Chem. Soc.* **1996**, *118*, 6317–6318.

4. Lazzeretti, P. *Phys. Chem. Chem. Phys.* **2004**, *6*, 217–223.

5. Steiner, E., Fowler, P. W. and Jenneskens, L. W. *Angew. Chem. Int. Edit.* **2001**, *40*, 362–366.

6. Gershoni-Poranne, R. and Stanger, A. *Chem. Soc. Rev.* **2015**, *44*, 6597–6615.

7. Krygowski, T. M. and Cyranski, M. K. *Chem. Rev.* **2001**, *101*, 1385–1420.

8. Matta, C. F. and Hernández-Trujillo, J. *J. Phys. Chem. A* **2003**, *107*, 7496–7504.

9. Poater, J., Fradera, X., Duran, M. and Solà, M. *Chem.-Eur. J.* **2003**, *9*, 400–406.

10. Matito, E., Duran, M. and Solà, M. *J. Chem. Phys.* **2005**, *122*, 014109.

11. Bultinck, P., Ponec, R. and Van Damme, S. *J. Phys. Org. Chem.* **2005**, *18*, 706–718.

12. Bultinck, P., Rafat, M., Ponec, R., Van Gheluwe, B., Carbo-Dorca, R. and Popelier, P. *J. Phys. Chem. A* **2006**, *110*, 7642–7648.

13. Poater, J., Duran, M., Solà, M. and Silvi, B. *Chem. Rev.* **2005**, *105*, 3911–3947.

14. Jug, K. and Köster, A. M. *J. Phys. Org. Chem.* **1991**, *4*, 163–169.

15. Katritzky, A. R., Karelson, M., Sild, S., Krygowski, T. M. and Jug, K. *J. Org. Chem.* **1998**, *63*, 5228–5231.

16. Katritzky, A. R., Barczynski, P., Musumarra, G., Pisano, D. and Szafran, M. *J. Am. Chem. Soc.* **1989**, *111*, 7–15.

17. Poater, J., García-Cruz, I., Illas, F. and Solà, M. *Phys. Chem. Chem. Phys.* **2004**, *6*, 314–318.

18. Bultinck, P. *Faraday Discuss.* **2007**, *135*, 347–365.

19. Stanger, A. *Chem. Commun.* **2009**, pages 1939–1947.

20. London, F. *J. Phys.-Paris* **1937**, *8*, 397–409.

21. Pople, J., In *Proceedings of the Royal Society of London A: Mathematical, Physical and Engineering Sciences* Vol. 239 pages 541–549. The Royal Society 1957.

22. Keith, T. A. and Bader, R. F. *Chem. Phys. Lett.* **1993**, *210*, 223–231.

23. Gomes, J. and Mallion, R. *Chem. Rev.* **2001**, *101*, 1349–1384.

24. Lazzeretti, P., Malagoli, M. and Zanasi, R. *Chem. Phys. Lett.* **1994**, *220*, 299–304.

25. Lazzeretti, P. *Prog. Nucl. Mag. Res. Sp.* **2000**, *36*, 1–88.

26. Geuenich, D., Hess, K., Kohler, F. and Herges, R. *Chem. Rev.* **2005**, *105*, 3758–3772.

27. Dauben, H. J., Wilson, J. D. and Laity, J. L. *J. Am. Chem. Soc.* **1968**, *90*, 811–813.

28. Steiner, E. and Fowler, P. W. *Phys. Chem. Chem. Phys.* **2004**, *6*, 261–272.

29. Minkin, V., Glukhovtsev, M. and Simkin, B. *Aromaticity and Antiaromaticity: Electronic and Structural Aspects* Wiley 1994.

30. Elser, V. and Haddon, R. C. *Nature* **1987**, *325*, 792–794.

31. Chen, Z., Wannere, C. S., Corminboeuf, C., Puchta, R. and Schleyer, P. v. R. *Chem. Rev.* **2005**, *105*, 3842–3888.

32. Fallah-Bagher-Shaidaei, H., Wannere, C. S., Corminboeuf, C., Puchta, R. and Schleyer, P. v. R. *Org. Lett.* **2006**, *8*, 863–866.

33. Cernusak, I., Fowler, P. and Steiner, E. *Mol. Phys.* **2000**, *98*, 945–953.

34. Corminboeuf, C., Heine, T., Seifert, G., Schleyer, P. v. R. and Weber, J. *Phys. Chem. Chem. Phys.* **2004**, *6*, 273–276.

35. Aihara, J. I. *Chem. Phys. Lett.* **2002**, *365*, 34–39.

36. Poater, J., Solà, M., Viglione, R. G. and Zanasi, R. *J. Org. Chem.* **2004**, *69*, 7537–7542.

37. Pelloni, S. and Lazzeretti, P. *J. Phys. Chem. A* **2011**, *115*, 4553–4557.

38. Pelloni, S., Monaco, G., Lazzeretti, P. and Zanasi, R. *Phys. Chem. Chem. Phys.* **2011**, *13*, 20666–20672.

39. Schleyer, P. v. R., Manoharan, M., Wang, Z.-X., Kiran, B., Jiao, H., Puchta, R. and van Eikema Hommes, N. J. R. *Org. Lett.* **2001**, *3*, 2465–2468.

40. Stanger, A. *J. Org. Chem.* **2006**, *71*, 883–893.

41. Gershoni-Poranne, R. and Stanger, A. *Chem.-Eur. J.* **2014**, *20*, 5673–5688.

42. Merino, G., Heine, T. and Seifert, G. *Chem.-Eur. J.* **2004**, *10*, 4367–4371.

43. Kleinpeter, E., Klod, S. and Koch, A. *Theochem-J. Mol. Struc.* **2007**, *811*, 45–60.

44. Karadakov, P. B. and Horner, K. E. *J. Phys. Chem. A* **2013**, *117*, 518–523.

45. Horner, K. E. and Karadakov, P. B. *J. Org. Chem.* **2013**, *78*, 8037–8043.

46. Karadakov, P. B. and Horner, K. E. *J. Chem. Theory Comput.* **2016**, *12*, 558–563.

47. Van Damme, S., Acke, G., Havenith, R. W. and Bultinck, P. *Phys. Chem. Chem. Phys.* **2016**, *18*, 11746–11755.

48. Jameson, C. J. and Buckingham, A. *J. Phys. Chem.* **1979**, *83*, 3366–3371.

49. Jameson, C. J. and Buckingham, A. *J. Chem. Phys.* **1980**, *73*, 5684–5692.

50. Soncini, A., Fowler, P., Lazzeretti, P. and Zanasi, R. *Chem. Phys. Lett.* **2005**, *401*, 164–169.

51. Pelloni, S. and Lazzeretti, P. *Theor. Chem. Acc.* **2007**, *118*, 89–97.

52. Cuesta, I. G., Merás, D., Sánchez, A., Pelloni, S. and Lazzeretti, P. *J. Comput. Chem.* **2009**, *30*, 551–564.

53. Lazzeretti, P. *High Resolution NMR Spectroscopy: Understanding Molecules and their Electronic Structures* **2013**, *3*, 209.

54. Lazzeretti, P., In *Applications of Topological Methods in Molecular Chemistry;* Springer 2016; pages 151–226.

55. Alonso, M. and Finn, J. *Physics* Pearson Prentice Hall 1992.

56. Ferraro, M., Lazzeretti, P., Viglione, R. and Zanasi, R. *Chem. Phys. Lett.* **2004**, *390*, 268–271.

57. Ferraro, M., Faglioni, F., Ligabue, A., Pelloni, S. and Lazzeretti, P. *Magn. Reson. Chem.* **2005**, *43*, 316–320.

58. Steiner, E. and Fowler, P. W. *J. Phys. Chem. A* **2001**, *105*, 9553–9562.

59. Frisch, M. J., Trucks, G. W., Schlegel, H. B., Scuseria, G. E., Robb, M. A., Cheeseman, J. R., Scalmani, G., Barone, V., Petersson, G. A., Nakatsuji, H., Li, X., Caricato, M., Marenich, A. V., Bloino, J., Janesko, B. G., Gomperts, R., Mennucci, B., Hratchian, H. P., Ortiz, J. V., Izmaylov, A. F., Sonnenberg, J. L., Williams-Young, D., Ding, F., Lipparini, F., Egidi, F., Goings, J., Peng, B., Petrone, A., Henderson, T., Ranasinghe, D., Zakrzewski, V. G., Gao, J., Rega, N., Zheng, G., Liang, W., Hada, M., Ehara, M., Toyota, K., Fukuda, R., Hasegawa, J., Ishida, M., Nakajima, T., Honda, Y., Kitao, O., Nakai, H., Vreven, T., Throssell, K., Montgomery, Jr., J. A., Peralta, J. E., Ogliaro, F., Bearpark, M. J., Heyd, J. J., Brothers, E. N., Kudin, K. N., Staroverov, V. N., Keith, T. A., Kobayashi, R., Normand, J., Raghavachari, K., Rendell, A. P., Burant, J. C., Iyengar, S. S., Tomasi, J., Cossi, M., Millam, J. M., Klene, M., Adamo, C., Cammi, R., Ochterski, J. W., Martin, R. L., Morokuma, K., Farkas, O., Foresman, J. B. and Fox, D. J. Gaussian 16 Revision A.03 2016.

60. Guest, M. F., Bush, I. J., Van Dam, H. J. J., Sherwood, P., Thomas, J. M. H., Van Lenthe, J. H., Havenith, R. W. A. and Kendrick, J. *Mol. Phys.* **2005**, *103*, 719–747.

61. Lazzeretti, P. and Zanasi, R. SYSMO Package (University of Modena) Additional routines for evaluation and plotting of current density by Steiner E., Fowler P., Havenith R.W.A and Soncini A. 1980.

62. Hunter, J. D. *Comput. Sci. Eng.* **2007**, *9*, 90–95.

63. Carion, R., Liégeois, V., Champagne, B., Bonifazi, D., Pelloni, S. and Lazzeretti, P. *J. Phys. Chem. Lett.* **2010**, *1*, 1563–1568.

64. Juselius, J. and Sundholm, D. *Phys. Chem. Chem. Phys.* **1999**, *1*, 3429–3435.

65. Pelloni, S. and Lazzeretti, P. *J. Phys. Chem. A* **2011**, *115*, 4553–4557.